

Multi-layered solid-PCM thermocline thermal storage concept for CSP plants. Numerical analysis and perspectives.

Short title: MLSPCM thermocline concept for CSP

P.A. Galione^{a,b}, C.D. Pérez-Segarra^a, I. Rodríguez^a, A. Oliva^{a,*}, J. Rigola^a

^a*Heat and Mass Transfer Technological Center (CTTC), Universitat Politècnica de Catalunya - BarcelonaTech,
ETSEIAT, Colom 11, 08222, Terrassa (Barcelona), Spain*

^b*Instituto de Ingeniería Mecánica y Producción Industrial (IIMPI), Universidad de la República (Udelar), Uruguay*

Abstract

Thermocline storage concept has been considered for more than a decade as a possible solution to reduce the huge cost of the storage system in concentrated solar power (CSP) plants. However, one of the drawbacks of this concept is the decrease in its performance throughout the time. The objective of this paper is to present a new thermocline-like storage concept, which aims at circumventing this issue. The proposed concept consists of a storage tank filled with a combination of solid material and encapsulated PCMs, forming a multi-layered packed bed, with molten salt as the heat transfer fluid. The performance evaluation of each of the prototypes proposed is virtually tested by means of a detailed numerical methodology which considers the heat transfer and fluid dynamics phenomena present in these devices. The virtual tests carried out are designed so as to take into account several charging and discharging cycles until periodic state is achieved, i.e. when the same amount of energy is stored/released in consecutive charging/discharging cycles. As a result, the dependence of the storage capacity on the PCMs temperatures, the total energy and exergy stored/released, as well as the efficiencies of the storing process are compared for the different thermocline, single PCM, cascaded PCM and multi-layered solid-PCM (MLSPCM) configurations. The analysis shows that the multi-layered solid-PCM concept is a promising alternative for thermal storage in CSP plants.

Keywords: Thermal Energy Storage, CSP, Phase Change Materials, Thermocline, Multi-Layered Solid-PCM, Numerical Analysis

*Corresponding author

Email addresses: pedrog@cttc.upc.edu, pgalione@fing.edu.uy (P.A. Galione), cttc@cttc.upc.edu (A. Oliva)

NOMENCLATURE

A	Surface area
A_t	Transversal area of tank
A_w	Internal surface area of tank's lateral wall
C_p	Specific heat at constant pressure
d_p	Diameter of filler PCM capsule/solid particle
e_{cap}	Capsule's shell width
ex	Exergy
f	Mass liquid fraction (PCM)
g	Gravity acceleration
h	Specific total enthalpy
h_{conv}	Convection coefficient
k	Thermal conductivity
k_{eff}	Effective thermal conductivity
L	specific latent enthalpy
m, \dot{m}	Mass and mass flux
n_{fm}	Number of filler particles/capsules in tank section
Nu	Nusselt number
N_r	Number of control volumes of one filler particle/capsule
N_x	Number of tank sections
p	Pressure
Pe	Péclet number
Pr	Prandtl number
r	Radial direction
R_{cond}	Thermal conduction resistance of capsule shell
R_{conv}	Convection resistance between fluid and capsule/solid filler
Re	Reynolds number
t	Time
T	Temperature
U_{amb}	Global heat transfer convection coefficient between the fluid and the ambient
v	Velocity magnitude
V	Volume

Δt	Time step
Δx	Tank section height
ϵ	Volume liquid fraction (porosity)
μ	Dynamic viscosity
ρ	Density

Superscripts and subscripts:

amb	ambient
cap	PCM capsule shell
f	fluid flow
fm	filler material (PCM or solid)
i	Index of tank section/control volume
$i \pm 1/2$	Index of tank section's face limiting i and $i \pm 1$
in	Tank inlet
j	Index of capsule/solid filler control volume
$j \pm 1/2$	Index of filler control volume's face limiting j and $j \pm 1$
l, liq	Liquid phase
out	Tank outlet
s, sol	Solid phase

Abbreviations:

CSP	Concentrated Solar Power
HTF	Heat Transfer Fluid
LCOE	Levelized cost of Electricity
MLSPCM	Multi-Layered Solid-PCM
PCM	Phase Change Material
TES	Thermal Energy Storage

1. Introduction

Thermal energy storage (TES) systems are an essential feature to make a major profit of solar energy. These systems allow using the thermal energy stored in hours of high solar radiation in times of lower radiation and higher energy demands, reducing the mismatch between the supply and demand. In solar power generation stations, the incorporation of TES systems produce an increase in system reliability and generation capacity, and a decrease of the levelized cost of electricity (LCOE) [1, 2].

For concentrated solar power plants (CSP) the current standard for thermal energy storage is the

two-tank molten salt system [3, 4], which make profit of the sensible energy changes of a heat transfer fluid (molten salt) under a temperature difference. In the search for investment costs reduction, different designs which result in lower container volumes or in the use of less and/or cheaper storage media have been proposed as alternatives. Some of these, making use of the materials sensible energy capacity, are the thermocline tanks [5, 6] and the concrete storage designs [7].

Thermocline storage system consists of a single tank, with a volume somewhat higher than one of the two-tank system, filled with a solid material forming a porous packed bed through which the heat transfer fluid (HTF) flows. Most of the tank volume is occupied by the solid, which acts as a sensible energy storage medium, and therefore less of the more costly HTF is needed when compared to an equivalent two-tank system. Different solid materials have been considered, such as quartzite rocks, granite, sand [5], asbestos-containing wastes [8], etc.

Thermocline tanks rely on the principle of thermal stratification, which occurs in a fluid having temperature gradients under the action of the gravitational force. The hot fluid, having a lower density than the cold fluid, is pushed upwards by the buoyancy force while the low temperature fluid is displaced downwards. Therefore, the hot fluid is placed in the upper part of a tank, while the colder fluid stays at the bottom. As a consequence, a vertical temperature gradient is formed which is called “thermocline”. The filler material helps in maintaining the thermal gradient, preventing possible mixing flows that may be present due to effects such as cooling through the walls (see for instance [9, 10]) or strong inlet flow currents [11].

Phase change materials (PCM) can also be used to store energy, using less storage material than would be used with a sensible energy storage medium, taking advantage of the latent energy changes during a phase change. The resulting storage device should be more compact, and hopefully cheaper, than one that only makes use of the sensible energy changes. Thermal storage devices using encapsulated PCMs have been studied as a form of thermal storage devices for CSP applications by several authors. Liu et al. [12] perform an extensive review of PCMs suitable to be used in TES for CSP plants and of heat transfer enhancement methods. Michels and Pitz-Paal [13] studied, experimentally and numerically, the performance of storage systems using vertical shell and tube heat exchangers with different PCMs enclosed between the shell and the tubes, with different melting points (cascaded PCM), for parabolic trough plants. Shabgard et al. [14] studied cascaded latent heat storage with gravity-assisted heat pipes for CSP. They performed numerical simulations using a thermal network model and evaluated thermal performance of the different designs after a single charge/discharge cycle. Nithyanandam et al. [15] numerically analyzed packed bed thermal storage with single encapsulated PCMs by studying their performance after a single charging/discharging cycles and after a periodic

41 cyclic state is reached. Parametric studies were performed and guidelines for designing latent ther-
42 mocline storage systems for CSP were established. Flueckiger et al. [16] studied thermocline storage
43 for solar power stations augmented with latent heat. They integrated their numerical model of the
44 thermocline into a system-level model for the CSP plant and evaluated the effect of the increase of
45 the storage capacity with latent heat. When compared against solid-filled thermocline, limitations in
46 the thermal performance of designs including a single PCM were observed, while some improvement
47 was obtained with some of the cascaded PCM configurations.

48 Moreover, combination of latent and sensible storage devices has been studied for CSP plants
49 with direct steam generation (DSG) [17], where a PCM storage unit is intended for vapor generation
50 (evaporation) and the sensible energy units for absorbing the sensible energy of the heat transfer fluid
51 (preheating and superheating).

52 One of the configurations that have received the most attention is that of packed beds. Many
53 numerical investigations of thermal storage in packed beds can be found in the literature. Ismail and
54 Stuginsky [18] performed a comparative analysis of different packed bed models used for sensible and
55 latent heat storage. Flueckiger et al. [19] reviewed different experimental and numerical studies on
56 thermocline tanks for solar thermal storage. On one hand, models for packed beds of solid materials
57 [6, 19, 20, 21] usually disregard the temperature gradients inside the particles. On the other hand, if
58 the bed consists of PCM capsules [15, 16, 22, 23], thermal gradients inside them may be significant
59 and are generally, but not always, taken into account. Karthikeyan and Velraj [24] performed a
60 comparison of three one-dimensional models for packed beds of PCM spherical capsules, where the
61 effect of considering the radial variation of temperature inside the capsules was tested. All these
62 models are based on discretizing the conservation equations for the heat transfer fluid and the filler
63 bed, and usually, several simplifying assumptions are made. Depending on the scope of the numerical
64 code, one-, two- or three-dimensional simulations can be performed. However, due to the significantly
65 higher computational costs associated with two- (e.g. [6, 20]) and three-dimensional (none found in
66 the literature) models, one-dimensional analysis is usually chosen for studying several working cycles
67 of TES systems [15, 16, 22, 23, 24].

68 In this work, a new concept of thermocline-like storage system is proposed, consisting in com-
69 bining low-cost solid and PCM filler materials, appropriately chosen and placed inside the tank in a
70 multi-layered manner. This concept, initially presented in a congress paper [25], has been called Multi-
71 Layered Solid-PCM (MLSPCM). The main idea behind MLSPCM configurations is the inclusion of
72 high and low melting-point PCMs as filler materials at the ends of the tank, close to the inlet/outlet
73 ports. In [25], the thermal performance of different MLSPCM designs was tested by means of a sim-

74 plified numerical model. Preliminary results indicated that MLSPCM configurations may reduce the
75 thermocline degradation occurring in the single-solid filled tanks and thus achieve a higher efficiency
76 in the use of the storage capacity.

77 Zanganeh et al. [26] recently studied a similar configuration using air as the heat transfer fluid,
78 in which a single PCM layer of high melting point was placed at the top of a packed bed of rocks.
79 They concluded that the PCM layer contributed to the stabilization of the outflow temperature but
80 did not have an effect on the thermal efficiency of the system. The evaluation was performed after
81 several charge/discharge cycles of the same duration.

82 In this work, a numerical model for evaluating the thermal behavior and optimizing the design
83 of packed bed systems is presented. The model considers axial thermal conduction within the heat
84 transfer fluid and an special treatment for the convective term of the energy equation, diminishing
85 the artificial numerical diffusion. Since the intention is to test both solid and PCM filler materials,
86 radial variation of temperature within particles/capsules is taken into account. Numerical experiments
87 are carried out in order to compare the thermal performance of the MLSPCM prototypes against
88 different existent thermocline-like designs, such as solid-filled thermocline, single encapsulated PCM
89 and cascaded PCM concepts. Several configurations are here analyzed, and the results are discussed in
90 detail. Thermal performance is evaluated after running several charge/discharge cycles, until a periodic
91 state is reached. Time operation of the processes (charge and discharge) are not fixed beforehand but
92 depend on the temperature of the fluid coming out of the TES, which is limited by some temperature
93 thresholds. The intention with this is to mimic the operating conditions of a real CSP plant, where
94 the solar receivers and power block impose certain limits to the temperature of the HTF. Thermal
95 evaluation is mainly based on terms of total energy storage, efficiency in the use total storage capacity,
96 proportion of PCM effectively changing phase and exergy outputs.

97 **2. Mathematical modeling and numerical implementation**

98 Mass, momentum and energy conservation equations have to be solved in order to be able to
99 simulate the thermal behavior of a thermocline-like tank. Some simplifying assumptions are made
100 and empirical correlations are used. The most relevant assumptions are:

- 101 1. One-dimensional fluid flow and temperature distribution (in the flow direction).
- 102 2. One-dimensional heat transfer in filler particles/capsules (radial direction).
- 103 3. Spherical shape of filler particles/capsules.
- 104 4. Constant density of both fluid and filler bed materials (solid and PCM).
- 105 5. Natural convection and contact melting inside the PCM capsules are neglected.

6. Heat conduction between different filler material particles/capsules is not considered.
7. Negligible radiation heat transfer.

The energy conservation equations are discretized using the Finite Volume Method (FVM). The tank is divided in N_x transversal cylindrical sections of height Δx (see Fig. 1a). In each tank section, a single representative particle/capsule needs to be simulated, as all are affected by the same fluid temperature due to the one-dimensionality assumption. This filler particle/capsule, assumed as spherical, is discretized in the radial direction in N_r control volumes, as shown in Fig. 1b.

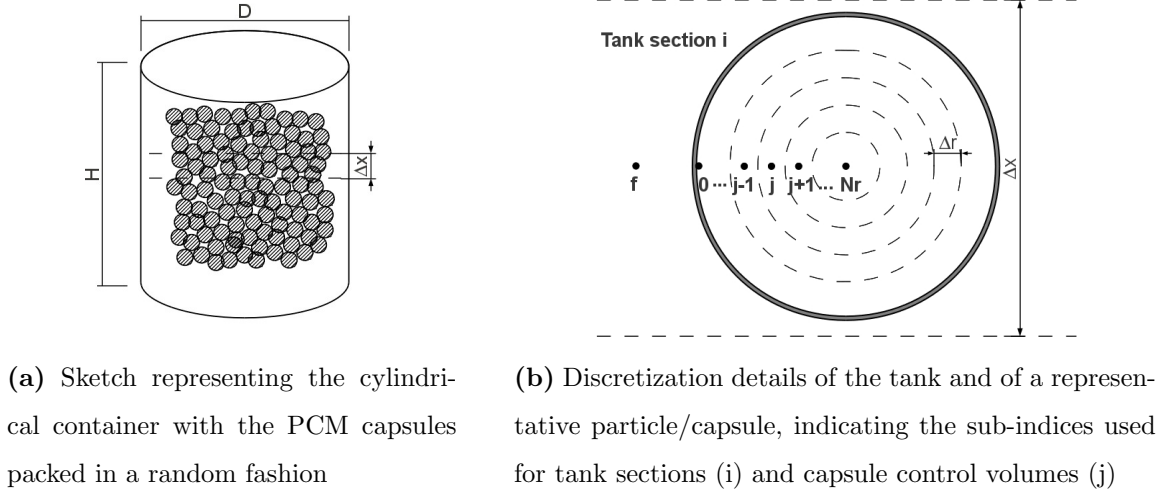


Figure 1: Domain and discretization

2.1. Energy

2.1.1. Heat transfer fluid (HTF)

The semi-discrete energy conservation equation of the fluid in the i^{th} tank section ($i = 1 \dots N_x$) results in:

$$\begin{aligned} \rho_f \epsilon_i V_i C_{p,f} \frac{\partial T_{f,i}}{\partial t} = A_t \left(k_{eff} \frac{\partial T_f}{\partial x} \right) \Big|_{i-1/2}^{i+1/2} - \dot{m} C_{p,f} (T_{f,i+1/2} - T_{f,i-1/2}) \\ - n_{fm,i} \frac{T_{f,i} - T_{i,0}}{R_{conv,i} + R_{cond,i}} - U_{amb} A_{w,i} (T_{f,i} - T_{amb}) \end{aligned} \quad (1)$$

where $T_{i,0}$ is the temperature of the internal surface of the particles/capsules (boundary node in fig. 1b). In the advective term (second in the right hand side) the fluid is assumed to be coming from section $i - 1$ and going to section $i + 1$. R_{cond} stands for the thermal resistance in the PCM capsules due to the capsule shell. The mass of the shell is disregarded here and is not considered to add any thermal inertia. The calculation of the thermal resistance due to convection between the HTF and the

filler material (R_{conv}) requires the fluid-to-bed Nusselt number, which is calculated using the following correlation, obtained from [27]:

$$Nu = 2.0 + 1.1Re^{0.6}Pr^{1/3} \quad \text{where } Re = \frac{\rho_f v_f d_p}{\mu_f} \quad (2)$$

As stated in [27], the correct use of Eq. (2) should take into account the effects of solid-phase conduction and thermal dispersion in the diffusive term [first term on the right hand side of Eq. (1)] and not only molecular diffusion. Therefore, the effective thermal conductivity is evaluated as follows:

$$k_{eff} = k_{eff}^0 + k_{eff}^{disp}$$

where the stagnant effective thermal conductivity (k_{eff}^0) is determined here as in [28]:

$$k_{eff}^0 = \left(\frac{k_{fm}}{k_f} \right)^{0.280 - 0.757 \log_{10}(\epsilon) - 0.057 \log_{10}(k_{fm}/k_f)} \quad (3)$$

and the effective conductivity due to thermal dispersion (k_{eff}^{disp}) is determined according to the following correlation [29]:

$$\frac{k_{eff}^{disp}}{k_f} = 0.00232Pe^2 \quad \text{where } Pe = RePr$$

In this work, some of the studied cases include one or several PCMs as filler materials. Since solid and liquid phases may have different thermal conductivities, a criterion is needed to determine the value of k_{fm} used in Eq. (3). The criterion adopted here consists in using the thermal conductivity calculated at the radius of capsule that divides the sphere in two parts of the same volume.

2.1.2. Filler material

The energy balance for the inner nodes ($j = 1 \dots N_r$) of the filler material remains:

$$\rho_f V_{i,j} \frac{\partial h_{i,j}}{\partial t} = \left(k_{fm} A \frac{\partial T}{\partial r} \right)_{i,j-1/2} - \left(k_{fm} A \frac{\partial T}{\partial r} \right)_{i,j+1/2} \quad (4a)$$

while for the boundary node ($j = 0$), in contact with the heat transfer fluid, results in:

$$\rho_f V_{i,0} \frac{\partial h_{i,0}}{\partial t} = \frac{T_{f,i} - T_{i,0}}{R_{conv,i} + R_{cond,i}} - \left(k_{fm} A \frac{\partial T}{\partial r} \right)_{i,1/2} \quad (4b)$$

In order to solve these equations it is necessary to define a relation between the enthalpy and the temperature of the filler materials. Considering constant specific heats for each phase, these relations are:

$$\begin{aligned}
h - h_0 &= C_{p,s}(T - T_0), & T &\leq T_s \\
h - h_0 &= C_{p,s}(T - T_0) + fL, & T_s &< T \leq T_{sl} \\
h - h_0 &= C_{p,l}(T - T_{sl}) + C_{p,s}(T_{sl} - T_0) + fL, & T_{sl} &< T \leq T_l \\
h - h_0 &= C_{p,l}(T - T_{sl}) + C_{p,s}(T_{sl} - T_0) + L, & T_l &< T
\end{aligned}$$

T_{sl} indicates the temperature in the phase change range chosen as the transition temperature for the specific energy from solid to liquid, or vice versa. Mass liquid fraction (f) values range from 0 (pure solid) to 1 (pure liquid), which, in this work, are calculated as a linear function of temperature in the phase change interval:

$$f = \frac{T - T_s}{T_l - T_s} \quad (5)$$

By taking a very narrow temperature range ($T_l - T_s$), fixed melting point PCMs can also be modeled with this approach. Hence, a unique value of h exists for each value of T , and the energy balance [Eq. (4)] may be expressed with T as the only variable. It should be noted that, since the location of the solid-liquid interface is implicitly determined by values of f , explicit tracking of interface is avoided with this strategy.

2.2. Momentum

To determine the pressure drop in the packed bed, the following momentum equation is solved:

$$\begin{aligned}
\left. \frac{\delta p}{\delta x} \right|_i &= \pm \left(\frac{5}{Re_{1,i}} + \frac{0.4}{Re_{1,i}^{0.1}} \right) \frac{6\rho_f v_f^2 (1 - \epsilon_i)}{d_{p,i} \epsilon_i^3} - \rho_f g \\
\text{where } Re_{1,i} &= \frac{\rho_f v_f d_{p,i}}{6(1 - \epsilon_i)\mu_f} \text{ (spherical particles) and } v_f = \frac{\dot{m}}{\rho_f A_t}
\end{aligned} \quad (6)$$

Eq. (6) is the Carman correlation for packed beds, which is generally used for solid objects forming a bed [30]. In this equation x increases from the bottom to the top, and therefore, the positive sign is used in the discharge of the tank while in the charge process the negative sign is used. The last term accounts for the pressure reduction/increase due to the gravitational action.

2.3. Exergy

For evaluating the power generating potential of the energy delivered by the thermal storage, the exergy global balance of the heat transfer fluid is calculated in the following manner:

$$\dot{m}(ex_{out} - ex_{in}) = \dot{m}C_{p,f}(T_{out} - T_{in} - T_{ref}\ln\frac{T_{out}}{T_{in}}) \quad (7)$$

where T_{ref} is the temperature corresponding to the dead state, which in this work has been taken as 45°C due to being a reasonable value for the temperature at which the vapor is condensed in the power generation block. The resulting exergy flow is the difference between the exergy exiting and entering the tank with the fluid.

2.4. Discretization details

Fully implicit schemes, such as that previously adopted in [25], may suffer from numerical diffusion in some degree. Since an accurate modeling of the temperature gradient is needed to evaluate the thermocline tank performance, a different method, similar to that presented by Oppel et al., [31], is used.

An upwind scheme with a first order explicit time integration has been adopted for the advective term, combined with the choice of a time step such that CFL=1 ($\Delta t = \epsilon\Delta x/u$). Therefore, each tank section is “filled” completely in each time step by the fluid coming from the upstream section with a temperature equal to the obtained in the previous time step. With this, if no damping is present (e.g. heat transfer to the filler material), a sharp temperature front is exactly transported from the inlet to the outlet with the velocity of the fluid flow. In cases where different porosities are present throughout the packed bed, different CFL numbers result for the same Δt . Here, CFL=1 has been enforced for the most restrictive zone (with the lowest porosity), and thus in the rest of the domain it has been maintained between 0 and 1, where some numerical diffusion is present. The physical diffusion in the HTF is modeled by the diffusive term in Eq. (1). A central difference spatial discretization and an explicit time integration have been adopted (although if the error in this term is significant, more than one iteration per time step is performed, which results in an approximation to an implicit time integration). To avoid instabilities and for accuracy reasons, the restriction in the time step by the diffusive term is: $\Delta t = 0.3(\epsilon\rho C_p\Delta x^2/2k_{eff})$. If the refinement of the grid is high, this limitation may be more restrictive than that of the convective term, and therefore, the CFL=1 condition is not applied anymore. For the diffusive terms of the filler energy equations [Eq. (4)], central differencing and fully implicit time integration have been adopted.

The algorithm used is similar to that indicated in [25], except that more than one iteration through the tank sections has been necessary at times, especially at the beginning of each process, in order to calculate more accurately the diffusive term. In each tank section (i), fluid and filler material temperatures have to be solved. The final matrix of coefficients derived from the system of equations

188 in each container section has a tri-diagonal pattern. This allows the usage of a TDMA algorithm to
 189 solve the linear system.

190 2.5. Model validation

191 The first case used to validate the model is that coming from the experimental work of Pacheco
 192 et al. [5]. There, a thermocline tank filled with quartzite rock and sand was tested, using molten
 193 salt as the heat transfer fluid. This case has been adopted as the validation case in several works on
 194 thermocline numerical modeling with solid and encapsulated PCM filler materials, see for instance
 195 [15, 16, 19, 20, 21].

196 The thermo-physical properties of the molten salt and of the mixture of quartzite rock and sand
 197 are indicated in Table 2. The HTF mass flow, which has been calculated following the same strategy
 198 as in [32], is set to 5.852 kg/s. The porosity is 0.22 and the effective particle diameter is 0.015 m.
 199 The initial state adopted in the simulations is the temperature map obtained from the experimental
 200 measures at time 11:30 [5]. Filler material and fluid inside the tank have been assumed to be at
 201 thermal equilibrium at this initial state.

202 The part of the tank containing solid filler material, of 5.2 m height, has been discretized axially in
 203 208 sections ($\Delta x = 2.5$ cm), while each simulated filler particle has been divided radially in 10 control
 204 volumes and the time step was set to $\Delta t \sim 12.45$ s (CFL = 1). These parameters have been verified
 205 in the sense of producing grid independent results (a difference of $\sim 0.1\%$ has been calculated against
 206 a case with 416 sections). Ambient losses have been neglected.

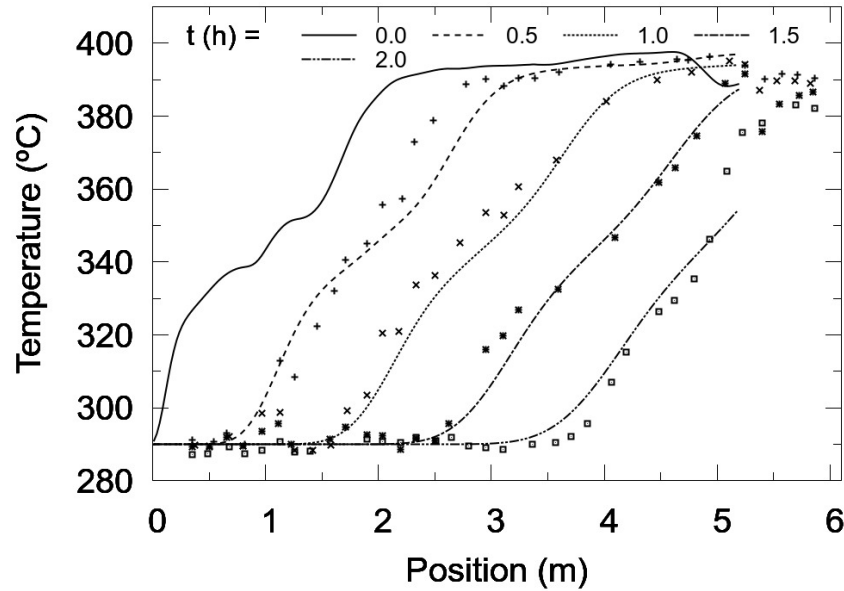


Figure 2: Validation. Solid lines correspond to the numerical results, while dots indicate the experimental results from Pacheco et al. [5]. The chronological order of the curves is from left to right.

Simulation results are presented in Fig. 2. It can be observed that the thermal gradient is well reproduced and that it moves towards the top as the discharge proceeds. Good agreement between experimental and numerical results is observed. The small discrepancies observed may be due to several causes, such as: uncertainties of the experimental measurements, unavailability of all the parameters from the original work of Pacheco et al. [5] and simplifications of the numerical model.

The second validation case corresponds to the charging of a tank filled with encapsulated PCM, from the experimental work of Nallusamy et al. [33]. All the configuration parameters and properties have been adopted from that work.

Figure 3 shows the results of evolution of temperature of the HTF (water) and PCM (paraffin melting at $60 \pm 1^\circ\text{C}$), measured at $x/L = 0.5$, where x is the axial position and L is the total height. In [33], the position inside the capsule at which the temperature is measured is not indicated. Numerical results of PCM temperatures shown in figure 3 are those obtained at the radius that divides the sphere in two parts of equal volume. Grid resolution for this case is $N_x = 92$ and $N_r = 55$, which has been checked for grid independence.

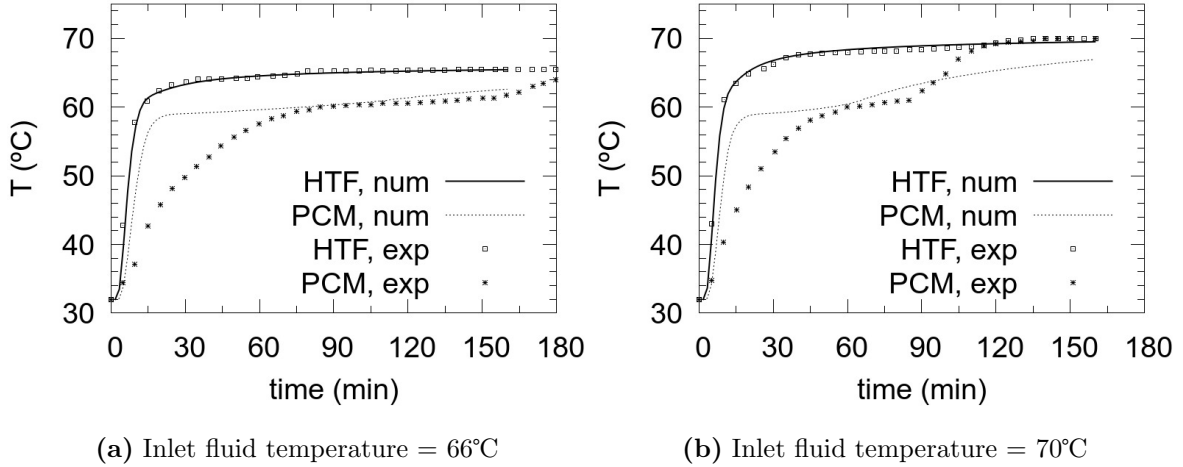


Figure 3: Temperature evolution at $x/L = 0.5$ of HTF and PCM. Experimental results, indicated by symbols, were extracted from [33]. Numerical results of PCM temperature are taken at the radius that divides the sphere in two parts of equal volume.

A good agreement is observed between experimental results (obtained from [33]) and numerical simulations, specially for the HTF. Some discrepancies are observed in the PCM temperatures. This is probably due to several reasons, such as not accounting for natural convection at the melting, differences between real thermo-physical properties and those used (paraffins have been observed to present high phase-change temperature ranges, as in [24], and thus melting probably starts at a lower temperature than that assumed) and uncertainty about the exact position of the temperature sensor. However, these discrepancies do not reflect significantly in the HTF temperature, for which

the agreement is very good.

3. Evaluation of different solutions

This section is devoted to the evaluation of thermocline tanks as thermal storage systems for CSP applications. The thermocline prototype tested by Pacheco et al. [5], is adopted as a reference case from which the operating conditions and tank global dimensions are taken.

Usually, in a CSP plant, the outlet temperature in the discharge process is limited by the minimum temperature that is admissible for the fluid feeding the power block. Similarly, for the charging process, the outlet temperature is limited by the restriction in the temperature of the fluid coming into the solar receivers. Therefore, both the operating time and the stored energy are determined by the level of temperatures attained by the outlet fluid in the charge and discharge processes.

Since the main objective is the evaluation of the performance of single thermocline-like tanks as storage devices in the context of a CSP plant, which is intended to be operated in charge/discharge cycles (one per day) during several years, this evaluation should not rely on values of energy (and exergy) stored or released in a single charge/discharge cycle. As the performance in a single charge (or discharge) process is highly dependent on the initial temperature distribution inside the tank, numerical experiments are carried out for several cycles until a periodic state—independent of the initial conditions of the first cycle—is achieved. Final performance values are determined at this state.

Furthermore, the substitution of all or part of the solid filler material by encapsulated PCM is considered. Therefore, tanks exclusively filled with an encapsulated PCM are tested, where the melting point has been taken as a parameter. Results obtained by the different choices of the melting point lead to the proposal of different combinations of “hybrid” thermocline configurations, in which both solid and encapsulated PCM filler materials are included. This new concept of thermocline-like storage system is herein called Multi-Layered Solid-PCM (MLSPCM). Fig. 4 shows a sketch of a MLSPCM configuration with 3 layers. Furthermore, cascaded PCM configurations are also tested and compared.

The same spatial discretization has been used for all the present cases, with 416 axial tank sections and 10 filler capsules/particles nodes. The difference with a coarser grid having 208 axial sections is less than 5% in all the cases, and therefore, the accuracy obtained is assumed to be good enough.

3.1. Study cases

The following operating conditions are assumed:

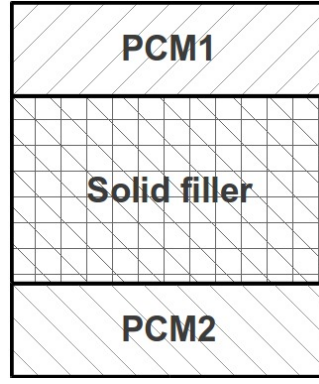


Figure 4: Sketch of a 3-layered MLSPCM configuration. PCM1 and PCM2 have high and low melting points, respectively.

- The geometry of the tank and operating conditions are the same for all the cases. Diameter of the filler particles/capsules is 15 mm. The porosity of the packed bed depends on the filler material and it is assumed to be 0.22 for the solid filler material and 0.34 for the encapsulated PCM. Moreover, a shell thickness of 0.4 mm is assumed for the PCM capsules.
- The operation time is not fixed. Instead, outlet temperature limits are imposed, which force the end of each process (charge or discharge) if the outflow temperature is not within these limits. These temperature intervals will be referred to as “admissible” temperature ranges. Here, both admissible ranges have been assumed to be 15% of the maximum temperature interval (100°C); i.e. in the charging phase, the outlet fluid temperature is allowed to be between 290°C and 305°C, while in the discharge it must be between 375°C and 390°C.
- Molten salt flow is fixed to 5.852 kg/s for both processes.
- Ambient losses are neglected [$U_{amb} = 0$ in Eq. (1)].
- Several consecutive charge/discharge cycles are simulated until a periodic thermal state is reached, i.e. when there is no variation of stored/released energy between consecutive cycles. Since ambient losses are neglected, in the periodic state the same energy that is stored in the charge must be released in the discharge.

As the admissible temperature intervals for both charge and discharge processes are quite narrow, outlet fluid temperatures for all the cases here studied are very similar. Therefore, a higher operation time is directly related to a higher stored (or released) energy.

In Table 1, a code for each case/configuration is defined. The presented cases can be classified according to the filler material/s used as: “pure” thermocline (A); single PCM (B); multi-layered

solid-PCM (C and D); and cascaded PCM (F). Percentages between brackets indicate the portion of total height occupied by each filler material. It should be noted that the chosen PCMs are fictitious, having the same thermal properties as those of potassium hydroxide (KOH) but with different fusion temperatures. The exception to this is case B1, where KOH is considered with its actual melting point (360°C according to [13]). This procedure has been adopted in order to account for the variations in performance exclusively due to the change in the fusion temperature of the PCMs. Figure 5 depicts sketches of some of the prototypes tested.

Table 1: Codification of cases.

Filler material ¹	Code
Quartzite rock & sand (Qu) (100%)	A
KOH (100%)	B1
KOH380 (100%)	B2
KOH300 (100%)	B3
MLSPCM: KOH380-Qu-KOH300 (20%-60%20%)	C1
MLSPCM: KOH380-Qu-KOH300 (40%-20%40%)	C2
MLSPCM: KOH380-Qu-KOH300 (10%-80%10%)	C4
MLSPCM: KOH380-Qu-KOH340-Qu-KOH300 (20%-20%-20%-20%-20%)	D1
MLSPCM: KOH380-Qu-KOH340-Qu-KOH300 (20%-25%-10%-25%-20%)	D2
KOH380-KOH370-KOH340-KOH310-KOH300 (32%-15%-6%-15%-32%)	F1
KOH380-KOH370-KOH340-KOH310-KOH300 (32%-9%-18%-9%-32%)	F2

^aMaterials KOHXXX (where XXX is a 3 digit number) are fictitious PCMs with fusion temperatures indicated by the number XXX (e.g. 300°C), whose thermal properties are equal to those of KOH (melting point = 360°C). The order in which the materials are indicated is the one in which they are placed inside the tank, from the top to the bottom. Between brackets, the proportion of the tank height occupied by each filler layer is indicated.

Table 2 shows the physical properties used in the simulations. Table 3 shows the mass of solid filler material, PCM and HTF contained. Due to the higher porosity of the PCM layers, more confined heat transfer fluid is contained in the configurations including encapsulated PCMs. Furthermore, as the solid filler material is denser than the PCM, prototypes including more of the former contain a higher total mass. The same table also presents data of the storage capacity for each configuration, i.e. the maximum amount of energy that could be stored taking into account both sensible and latent energy contributions, with a temperature jump equal to the difference between the hot and cold inlet fluid temperatures of charge and discharge processes, respectively. Here, the maximum temperature

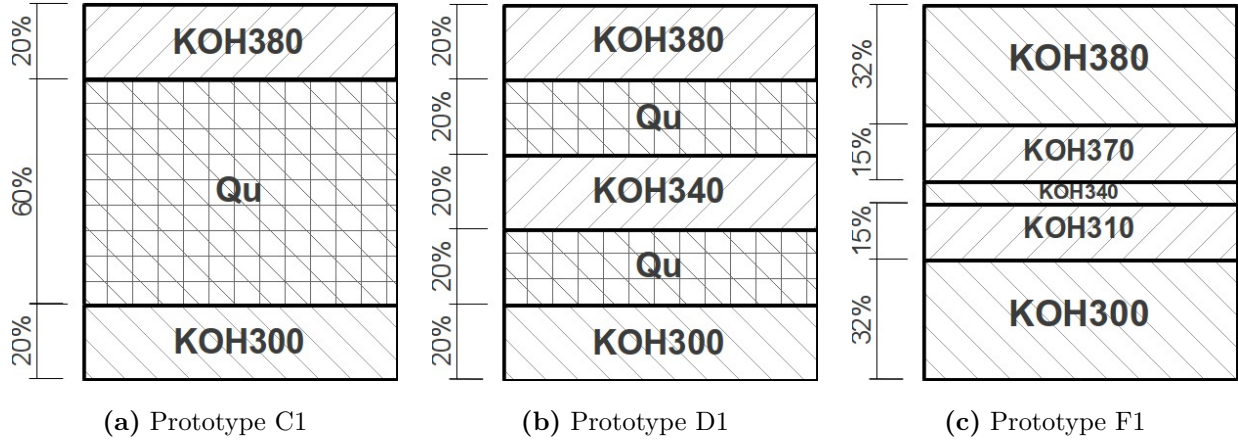


Figure 5: Sketches of some of the different filler configurations tested.

Table 2: Thermo-physical properties.

	Quartzite rock & sand (Qu) [20]	PCM (KOHXXX) [13]	Molten Salt (HTF) [34]
ρ (kg/m^3)	2500	2040	1873.8
$C_{p,s}$ ($J/kg K$)	830	1340	-
$C_{p,l}$ ($J/kg K$)	-	1340	1501.5
k_s ($W/m K$)	5.69	0.5	-
k_l ($W/m K$)	-	0.5	$0.443 + 1.9 \times 10^{-4}T(^{\circ}C)$
μ ($Pa s$)	-	-	$22.714 \times 10^{-3} - 0.12 \times 10^{-3}T +$ $2.281 \times 10^{-7}T^2 - 1.474 \times 10^{-10}T^3$
L (J/kg)	-	1.34×10^5	-

295 difference is $100^{\circ}C$ ($290^{\circ}C$ - $390^{\circ}C$). It can be observed that, even in the cases where the filler material is
 296 only encapsulated PCM (cases B1-3 and F1-2), the sensible energy capacity is higher than the latent
 297 one. This is due basically to two reasons: first, the temperature jump is relatively high, making the
 298 sensible energy capacity of the PCMs to be equal to their latent energy capacity ($C_p\Delta T = L$); and
 299 second, the HTF confined inside the tank contributes with an extra sensible energy capacity.

Table 3: Mass confined inside the tank and storage capacity.

Mass data (ton)	A	B1	B2	B3	C1	C2	C4	D1	D2	F1	F2
Mass of PCM	0.0	42.0	42.0	42.0	17.0	33.9	8.5	25.0	21.0	42.0	42.0
Mass of solid filler material	71.7	0.0	0.0	0.0	42.7	13.8	57.2	28.9	35.8	0.0	0.0
Mass of confined HTF	15.2	23.4	23.4	23.4	18.5	21.8	16.8	20.1	19.3	23.4	23.4
Total mass	86.8	65.4	65.4	65.4	78.2	69.5	82.5	74.1	76.1	65.4	65.4
Storage Capacity											
Filler material (MWh)	1.65	3.13	3.13	3.13	2.25	2.84	1.95	2.53	2.39	3.13	3.13
Confined HTF (MWh)	0.63	0.98	0.98	0.98	0.77	0.91	0.70	0.84	0.80	0.98	0.98
Total (filler + HTF) (MWh)	2.28	4.10	4.10	4.10	3.02	3.75	2.65	3.37	3.19	4.10	4.10
Total sensible energy (%)	100.0	61.9	61.9	61.9	79.1	66.4	88.1	72.3	75.5	61.9	61.9
Total latent energy (%)	0.0	38.1	38.1	38.1	20.9	33.6	11.9	27.7	24.5	38.1	38.1

3.2. Results and discussion

3.2.1. Case A: Solid filler material

Table 4 shows the thermal performance results for each case. Case A (“pure” thermocline) is shown to behave quite poorly in terms of stored energy when compared against the rest of the cases (with exception of case B1). The stored energy at thermal equilibrium is 1.45 MWh, which is around 63% of the storage capacity. This somewhat low efficiency is due to the thermocline degradation throughout the several charging-discharging cycles, enforced by the assumed temperature thresholds.

Table 4: Performance results for each configuration

Results	A	B1	B2	B3	C1	C2	C4	D1	D2	F1	F2
Operation time (h) ¹	1.67	1.16	2.61	2.62	2.86	2.99	2.68	1.82	3.00	3.28	2.03
Stored Energy in Filler material (MWh)	1.05	0.63	1.42	1.43	1.72	1.71	1.65	1.11	1.83	2.00	1.25
Stored Energy (Filler + confined HTF) (MWh)	1.45	1.00	2.19	2.20	2.32	2.42	2.22	1.48	2.43	2.66	1.64
Stored Energy / Storage capacity (%)	63.4	24.5	53.4	53.5	76.9	64.5	83.7	43.8	76.2	64.9	40.0
Sensible energy stored / Total stored (%)	100.0	96.3	90.7	90.7	80.0	80.0	86.7	69.8	73.7	64.0	60.6
Latent energy stored / Total stored (%)	0.0	3.7	9.3	9.3	20.0	20.0	13.3	30.2	26.3	36.0	39.4
Effective mass of PCM changing phase (%)	-	2.4	13.1	13.1	73.6	38.4	93.2	47.9	81.7	61.3	41.4
Exergy difference at charge (MWh)	-0.70	-0.48	-1.05	-1.06	-1.12	-1.17	-1.07	-0.71	-1.18	-1.29	-0.79
Exergy difference at discharge (MWh)	0.69	0.48	1.04	1.05	1.11	1.15	1.06	0.70	1.16	1.27	0.78
Pressure losses due to filler bed (Pa)	< 400	< 100	< 100	< 100	< 250	< 150	< 350	< 200	< 250	< 100	< 100

^aIn cases where the charge and discharge operation times are different, (e.g. B2 and B3) the mean value between processes is shown.

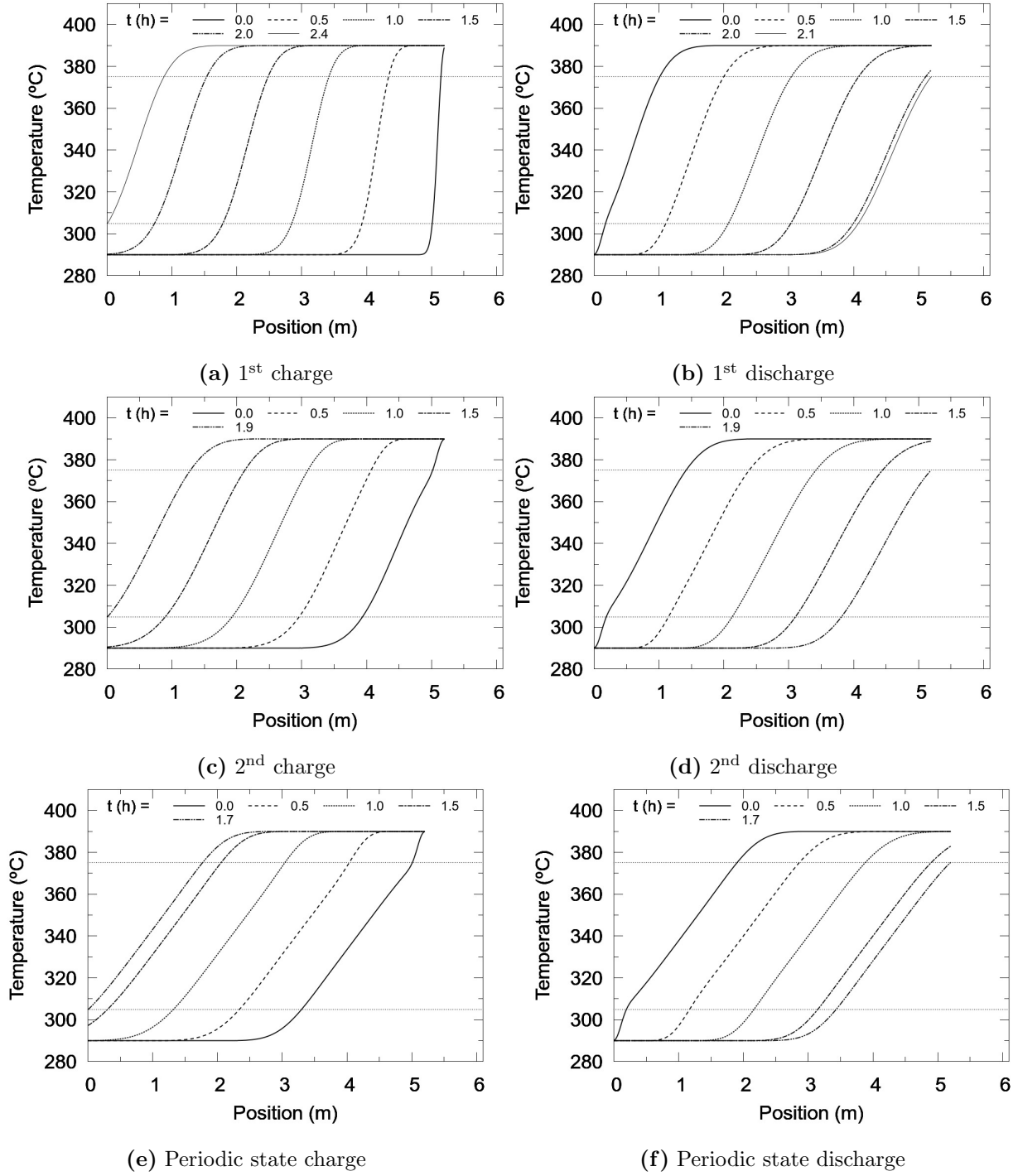


Figure 6: Case A. Temperature maps at various instants for the first two cycles and the periodic state. The chronological order of the curves is from left to right in the charge and from right to left in the discharge.

Figure 6 shows the temperature maps obtained for case A, of charge and discharge processes at various instants for the first two cycles and the periodic state. The degradation of the thermocline can be clearly observed by comparing the 1st and last cycles. The initial condition in the first charge process is a uniform cold temperature throughout the tank. For the 2nd cycle, the initial condition of

the filler material and HTF is not anymore a uniform temperature curve, but one with the temperature gradient resulting from the last discharge process. This change in the initial conditions is inevitable due to the requirements imposed on the outgoing fluid temperature, which enforce it to lie inside the admissible range. Since the difference between the incoming fluid temperature and that of the filler material is lower than in the 1st charge process, the heat transfer rate, and thus the thermal gradient (in absolute value), are also lower in the 2nd charging.

Therefore, during the consecutive charging/discharging cycles, the thermal gradient tends to get “flattened” until a periodic unsteady state is reached. Due to this thermocline degradation, the stored/released energy in this periodic state is lower than those of the previous cycles, and so is the operation time, since outlet thresholds are reached earlier.

A useful way of estimating the stored/released energy in each process is to calculate the area between the initial temperature map and the last one, since sensible energy differences are proportional to the temperature jumps. From the comparison between figures 6a and 6e, a clear difference can be observed in the area between initial and last temperature maps of the charge processes.

Once the periodic state is reached, symmetry between processes can be observed; and therefore, the energy which is stored in the charge is later delivered in the discharge. This is due to having disregarded the thermal losses to the ambient.

3.2.2. Cases B1-3: Encapsulated PCM

A first look into the storage capacity values of Table 3 can induce the reader to think that a storage tank filled with an encapsulated PCM should store more energy than the same tank filled with a solid filler material. However, results shown in Table 4 reveal a different situation.

Prototype of case B1 is filled with a single encapsulated PCM with a fusion temperature of 360°C (KOH), which is well between the operating temperatures of the storage system.

The temperature maps of the HTF inside the tank at various instants for the first two and periodic state cycles, are plotted in figure 7. A clear picture of the problem results from their observation. In the first charge, with an initially cold tank, the outlet temperature threshold is reached in a moment where only part of the contained PCM capsules have melted. The position inside the tank where the phase-changing capsules are located, can be identified by the location where there is a steep temperature gradient ranging from 390°C to 360°C, which for the final state is located at a distance of around 3.6 m from the bottom. Therefore, only a portion of the available latent heat has been used. Moreover, the sensible energy capacity of both the PCM and HTF is much less harnessed than in case A. Thus, the initial condition for the subsequent discharge is one where only a part of both the latent and sensible energy capacity can be exploited.

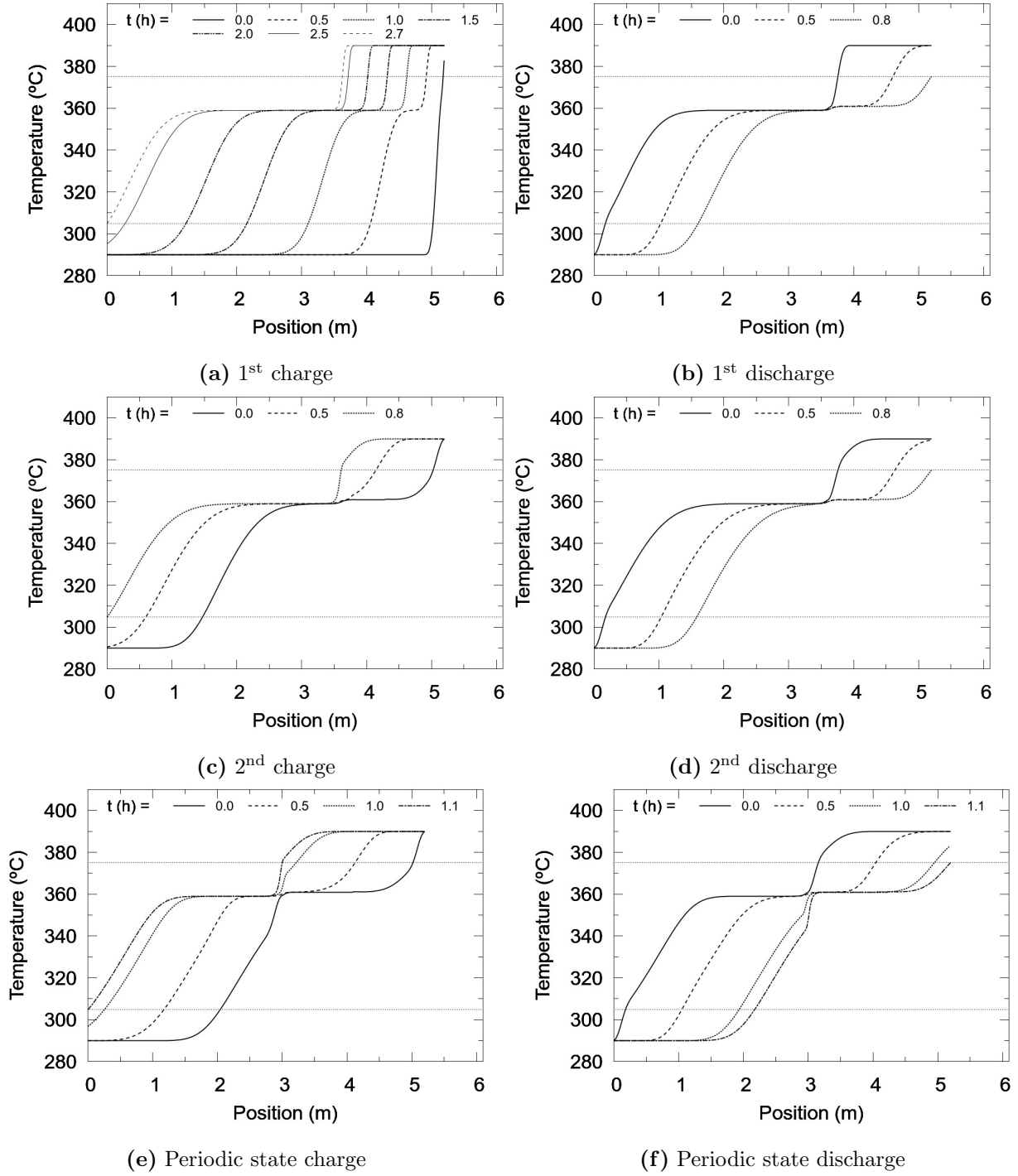


Figure 7: Case B1. Temperature maps at various instants for the first two and last cycles. The chronological order of the curves is from left to right in the charge and from right to left in the discharge.

An important observation is that the melting point of KOH lies outside the admissible temperature ranges for both charging and discharging processes. In the figure it can be observed how the temperature of the HTF passing through the phase-changing PCM capsules is kept close to their melting point. Therefore, in the charging phase, the filler material located downstream of the phase-changing

capsules receive the HTF with a temperature equal to the melting point, not being able to melt. Since the threshold temperature is lower than the melting point, the charging process ends before all the PCM has melted, when the capsules located at the outlet (top) cannot bring the HTF temperature below the threshold, with the use of their sensible energy capacity alone.

At the periodic state, the area between the initial and last temperature curves is somewhat higher than those corresponding to the initial cycles (except from the 1st charge). Furthermore, the location of the phase-changing layers has been shifted slightly to the center of the tank.

Cases B2 and B3 have the common feature of using PCMs whose melting points lie inside each of the admissible temperature ranges. In B2 a melting point of 380°C has been chosen, which is inside the admissible range for the outlet fluid temperature of the discharging process (375°C- 390°C); while a melting point of 300°C has been chosen for case B3, lying inside the admissible range of the charging process (290°C- 305°C).

Temperature maps for the periodic state of both cases are shown in figures 8 and 9. A first observation is that the area between the initial and final maps for both cases is higher than that of case B1. As a result, a higher energy is stored in both cases, as can be observed in Table 4.

In these cases, due to the more “intelligent” choice of the melting points, a higher utilization of the whole storage capacity has been attained. For example, in case B2, as the cold fluid comes through the bottom of the tank and the thermal gradient travels to the top, the layers of PCM located at the hot zone, which have melted in the previous charging, act as thermal “buffers” for the outgoing fluid, keeping its temperature close to the melting point until almost all the PCM near the outlet has solidified. Since this temperature is inside the admissible range, the process does not stop, and the rest of the upstream filler material can be thermally discharged.

Due to the symmetry between key temperatures of cases B2 and B3 (melting points, thresholds and operating range), the resulting temperature maps for the periodic state are also symmetric. Charging process of case B2 looks the same as the discharging process of B3, with a shift of the sense in which both axis increase. Furthermore, the results of both cases shown in Table 4 are almost identical.

However, a slight difference is encountered in the value of exergy delivered in the discharging phase. Result for case B3, with a PCM melting point of 300°C is slightly higher than that of case B2, where a melting point of 380°C has been adopted. This result may seem strange, since one could think that a higher melting point of the PCM should result in a higher amount of hot fluid coming out of the tank and a higher amount of exergy delivered in the discharge. The explanation for this result can also be extracted from the temperature maps shown in figures 8 and 9. In case B2, the temperature of the outgoing fluid in the discharge is seen to be the PCM melting point during most of the process

(Fig. 8b); while in case B3, it is observed that during most of the discharging phase, the outlet fluid temperature is the maximum possible (Fig. 9b). The reason for this is that the low melting point PCM, acting as a thermal buffer during the charging phase, allows the upstream filler material to be charged of sensible energy up to the maximum temperature, while the high melting point PCM of case B3 is storing most of the high temperature energy (between 380°C and 390°C) in the form of latent heat at 380°C. On the other hand, case B2 also stores less exergy than case B3, since it needs less time to be charged (see figures 8a and 9a), and its final exergy efficiency (delivered/stored) is slightly higher in the former.

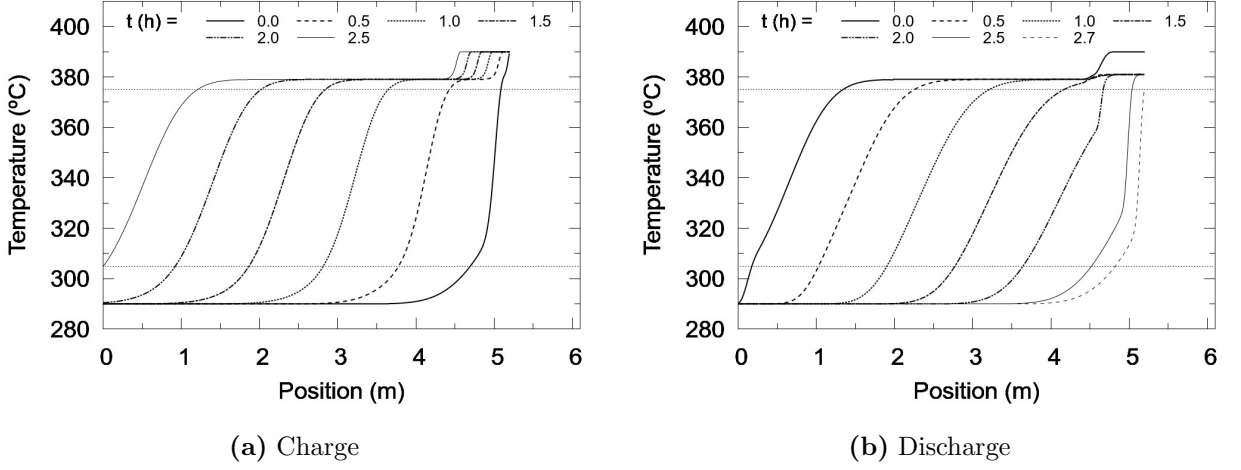


Figure 8: Case B2. Periodic state. Temperature maps at various instants. The chronological order of the curves is from right to left for the charge process and from left to right for the discharge.

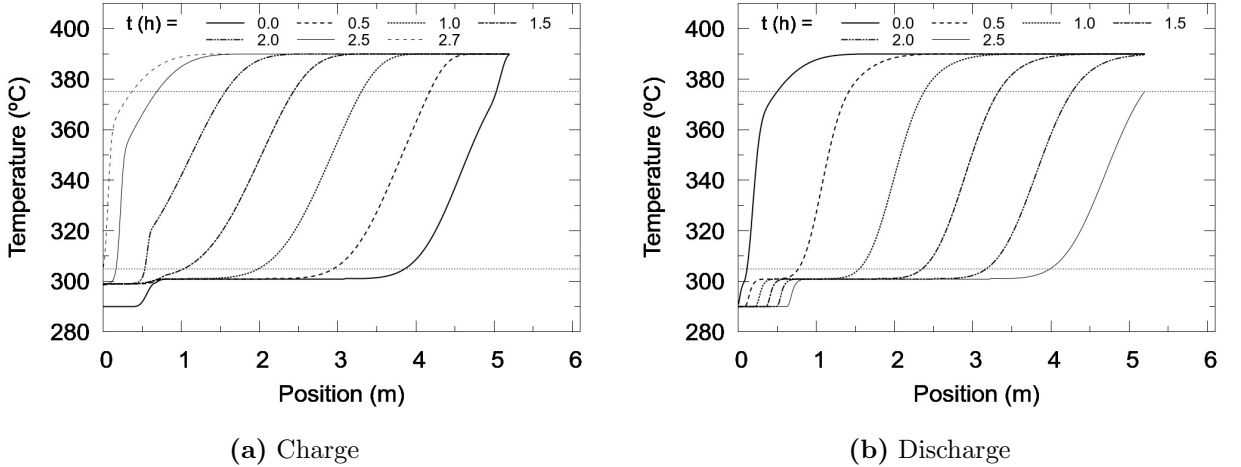


Figure 9: Case B3. Periodic state. Temperature maps at various instants. The chronological order of the curves is from right to left for the charge process and from left to right for the discharge.

3.2.3. Cases C1-3, D1-2: Multi-layered solid-PCM (MLSPCM)

Results obtained with cases B1 - B3 show that even in the best case, only a little amount of PCM is effectively changing phase in a cycle (less than 15%). Moreover, the results of cases B2 and B3 show that an effective way of increasing the stored energy of an encapsulated PCM tank is to choose a PCM whose fusion temperature lies between an admissible temperature interval for either one of the processes (charge or discharge). Thus, the PCM capsules located at the end of the tank, where the HTF temperature is close to its melting point, act as a thermal buffer maintaining a desirable outlet temperature, while the rest of the tank is charged (or discharged) with sensible energy.

Therefore, a tank which is filled with PCM in such a way that most of it can effectively undergo through the phase change, together with the inclusion of a cheaper solid filler material to store the sensible energy, should be a much more efficient and cost-effective thermal storage device.

Hence, all the configurations studied in this section contain PCM layers at both extremes, one with a high melting point placed at the top of the tank (hot zone) and another with a low melting point placed at the bottom (cold zone), together with solid filler material placed in between.

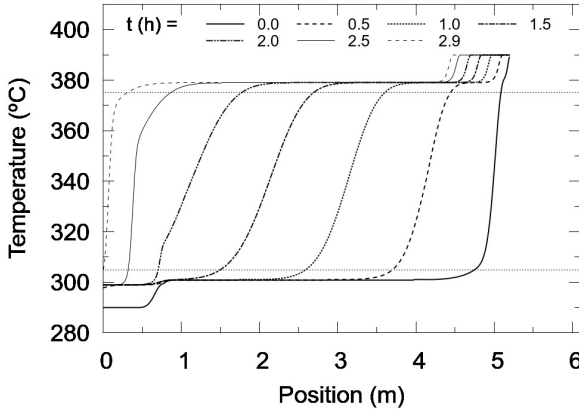
The symmetry of the proposed problem, given the operation conditions, induces to design the multi-layered prototypes using symmetric configurations, i.e. using the same width for the PCM layers whose melting point are at the same distance (in temperature units) from the corresponding outlet temperatures.

Cases C1 (see sketch on Fig. 5a), C2 and C4 are MLSPCM configurations with only two different PCMs collocated at both extremes of the tank and a solid filler material (quartzite rocks & sand) in the middle zone, forming a 3-layer arrangement, only differing in the width of the layers. PCMs used are those of cases B2 (KOH380) and B3 (KOH300), having melting points lying inside the corresponding admissible range.

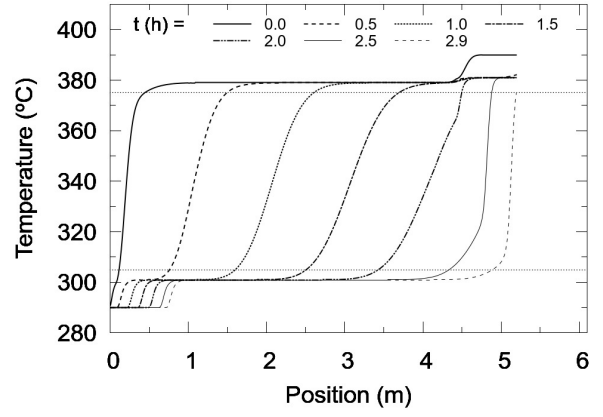
Performance results of the three cases, in Table 4, show a significant improvement with respect to cases A and B1-3. The “buffering” effect of the PCM at both ends can be appreciated in figures 10 to 12. An increase in the amount of stored/released energy in the periodic state is observed. The efficiency in the usage of both the total thermal capacity and the latent energy capacity are also higher.

C2 stores the highest amount of energy of the three, but is the one with the lowest efficiencies in terms of utilization of both total and latent storage capacities. In fact, C4, with the least amount of PCM, is the best in terms of efficiency. Around 93% of the PCM is effectively changing phase between successive processes in the latter case, while 74% is the corresponding value for C1 and 38% for C2. In terms of total storage, C1 stores around 4% less than C2, while C4 is around 8% worse than C2.

Regarding the values of fraction of energy stored in the form of latent heat, it can be observed

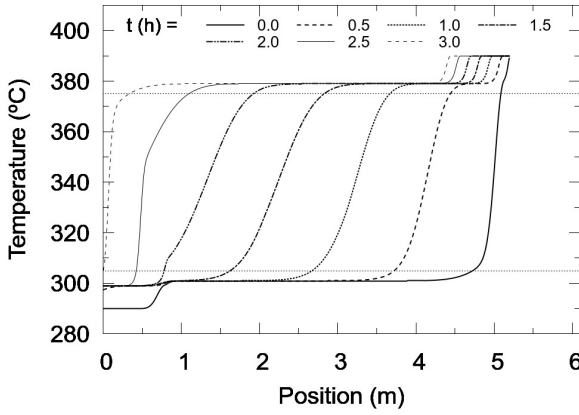


(a) Charge

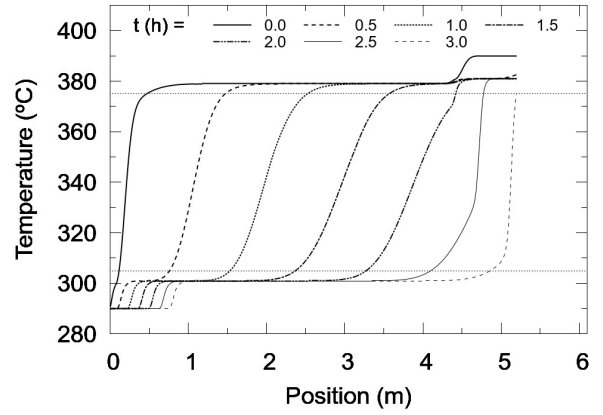


(b) Discharge

Figure 10: Case C1. Periodic state. Temperature maps at various instants. The chronological order of the curves is from right to left for the charge process and from left to right for the discharge.



(a) Charge



(b) Discharge

Figure 11: Case C2. Periodic state. Temperature maps at various instants. The chronological order of the curves is from right to left for the charge process and from left to right for the discharge.

that for cases C1 and C2 they are almost exactly the same and lower for case C4. This can be explained by the following reasoning. The available energy for storage, from the HTF, is in the form of sensible energy and thus, it is proportional (with the approximation of having constant specific heat) to the temperature difference. Therefore, from the point of view of the high melting point PCM, melting at 380°C, the energy contained in the HTF which is available for being stored in the melting process, is only that between 380°C and 390°C. This is only 10% of the energy contained in the HTF between 290°C and 390°C, and 11.7% of that between 305°C and 390°C (considering both limits of the admissible range of outlet HTF temperatures in the charge). This means that, at most, only 10%-12% of the energy that needs to be extracted from the HTF can be used for melting this PCM, given the constraint for the outgoing temperature of not surpassing 305°C.

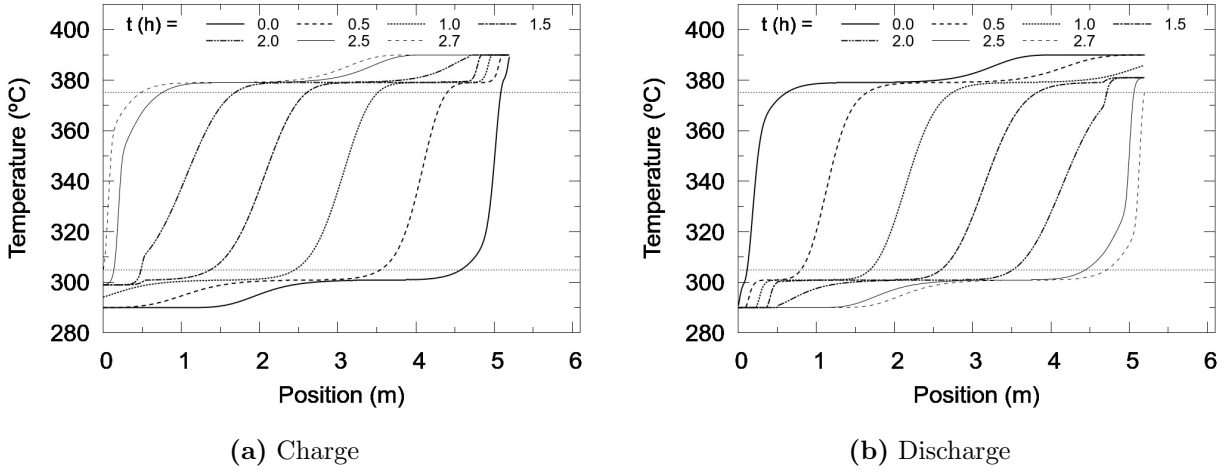


Figure 12: Case C4. Periodic state. Temperature maps at various instants. The chronological order of the curves is from right to left for the charge process and from left to right for the discharge.

It could be argued that, having a second PCM placed at the outlet with a much lower melting point (300°C), much more energy could be stored in the form of latent heat, since the energy contained in a much broader range of temperatures is available for melting this other PCM (in the case of total utilization of the first 10% for melting the first PCM, this range would be 300°C – 380°C ; or less, if the sensible energy stored in the layers upstream from the second PCM is considered). However, this is not the case when the periodic state has been reached. In this state, and in the absence of thermal losses, the energy stored in the charge is the same as that delivered in the subsequent discharge. Furthermore, the same amount of PCM that melts in the charge, is solidified in the next discharge. For this reason, if 10% of the total available energy is used to melt the high melting point PCM, then only this same amount will be delivered by it in the subsequent discharge. Given the symmetry of the problem, the same reasoning can be applied to the low melting point PCM.

Therefore, as each PCM layer can only theoretically store around 10% - 12% of the total available energy, both PCMs can sum up to 20% - 24% of it, at most. Case C1 and C2 both result in a latent storage of 20%. C4, having significantly less amount of PCM, only reach to around 13%. Table 3 shows that the latent capacity of prototype C1, C2 and C4 is around 21%, 34% and 12%, respectively. This is the reason why in case C2 only a small fraction of the PCM effectively changed phase, having a higher latent heat capacity fraction than the theoretically possible.

Cases D1 (see sketch in Fig. 5b) and D2 consist of 5-layered MLSPCM tanks. Both PCM layers at the ends are maintained, while an extra PCM layer is added in the middle zone, with a melting point equal to the mean temperature of the operation range, i.e. 340°C . Other two solid filler material layers are placed between the PCM layers.

Case D1 is seen to behave worse than the previous C1-3 cases. Figure 13 shows the temperature maps obtained for this case, with a similar behavior to that of B1. The presence of KOH340 acts as a thermal buffer keeping the HTF temperature close to its melting point, which is outside both admissible temperature ranges. The thermal buffering provided by the other two PCMs is not enough to allow it to melt and solidify completely before the end of the charge and discharge processes, causing the melting point of 340°C to be a limit to the temperature jump of the solid filler layers and also of much of the middle PCM layer. As a result, the stored energy and the efficiencies are much worse than those of the previous MLSPCM prototypes.

On the other hand, case D2, with the only difference of containing a middle layer of half the width compared to D1, results in a significantly different behavior. Figure 14 shows the temperature maps obtained for this case, where a behavior similar to that of cases C1 and C2 can be observed. Here, the thermal buffering effect of the middle layer does not last so long and the top and bottom PCM layers are capable of bearing the “extra” exigency. In fact, the inclusion of the middle layer has resulted in an overall increase in the stored energy with almost the same efficiency, compared to case C1, which had a lower amount of PCM effectively changing phase.

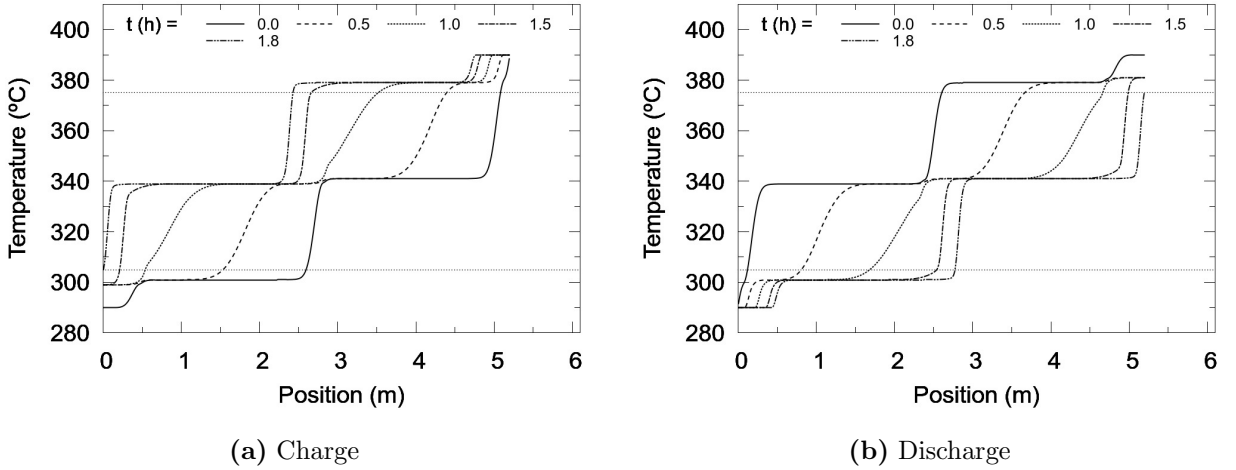


Figure 13: Case D1. Periodic state. Temperature maps at various instants. The chronological order of the curves is from right to left for the charge process and from left to right for the discharge.

3.2.4. Cases F1-2: Cascaded PCMs

In the cascaded PCM configurations considered here, as in MLSPCM cases, PCM layers located at both ends with melting points lying inside the admissible ranges are included.

The difference between these prototypes and MLSPCM ones, is that no solid filler material is included in the formers. Instead, several layers of different PCMs are placed inside the tank, with increasing melting points from the bottom to the top. This kind of configuration has been studied by

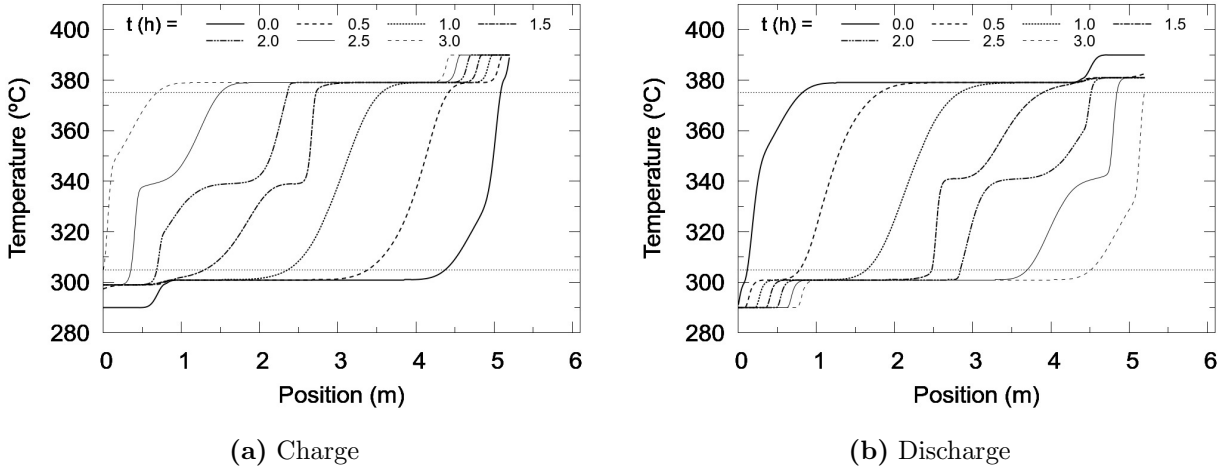


Figure 14: Case D2. Periodic state. Temperature maps at various instants. The chronological order of the curves is from right to left for the charge process and from left to right for the discharge.

other authors, e.g. Michels and Pitz-Paal, [13]. A sketch of configuration F1 is depicted in figure 5c.

The difference between F1 and F2 is in the width of the three middle layers, where the PCMs with melting points outside the admissible ranges are located. Case F1 includes more of the PCMs with melting points more near the admissible limits (KOH370 and KOH310), while F2 includes more of the middle PCM with a temperature equal to the operating temperatures mean value (KOH340).

Results of Table 4 show that the performance of case F1 is significantly better than that of case F2. As both cases use the same PCM layers, the difference between them is only due to the different proportion of materials included. Temperature maps of both cases at the periodic state can be observed in figures 15 and 16. Significant differences are encountered. In case F1, the temperature range traversed by the fluid inside the tank is sensibly higher than in case F2. In case F1, when the PCM at the ends have almost completely changed of phase—maintaining outlet fluid temperature inside the admissible range—a considerable amount of the PCM layers inside the tank have also melted/solidified. This is not what happens in case F2, for which the outlet fluid temperature cannot stay within the admissible ranges enough time to allow a good utilization of sensible and latent capacities. Hence, as it has been observed with MLSPCM cases, a correct design of the PCM layers is a critical aspect in the final performance.

Case F1 has been the best of all the studied cases in thermal storage capacity. The energy stored is around 15%, 10%, 20% and 9% higher than for cases C1, C2, C4 and D2, respectively. However, the efficiency in the use of the storage capacity is not very high (65%), with 61% of the PCM effectively changing phase.

Some other cascaded PCM cases with different layer thicknesses have been tested (not presented),

with the result of F1 being the best of all. It might be possible to find other arrangements, with the same PCM layers, with better performance, although it is the authors belief that this arrangement is close to the best possible results.

Considering that an encapsulated PCM is probably much more costly than the solid filler material, MLSPCM prototypes can be expected to be more cost-effective than cascaded PCM, also considering the better efficiency of the former in the use of PCMs latent heat.

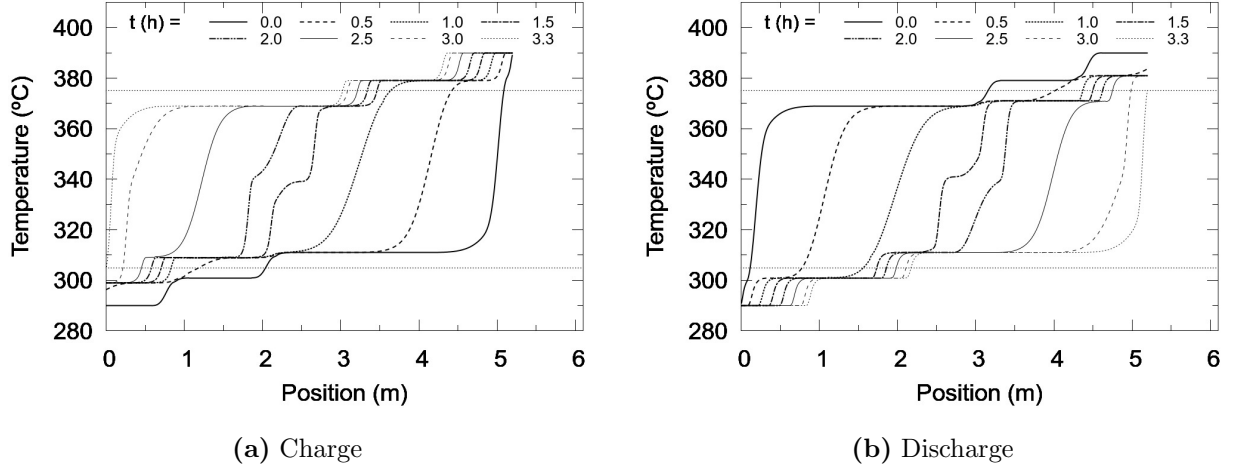


Figure 15: Case F1. Periodic state. Temperature maps at various instants. The chronological order of the curves is from right to left for the charge process and from left to right for the discharge.

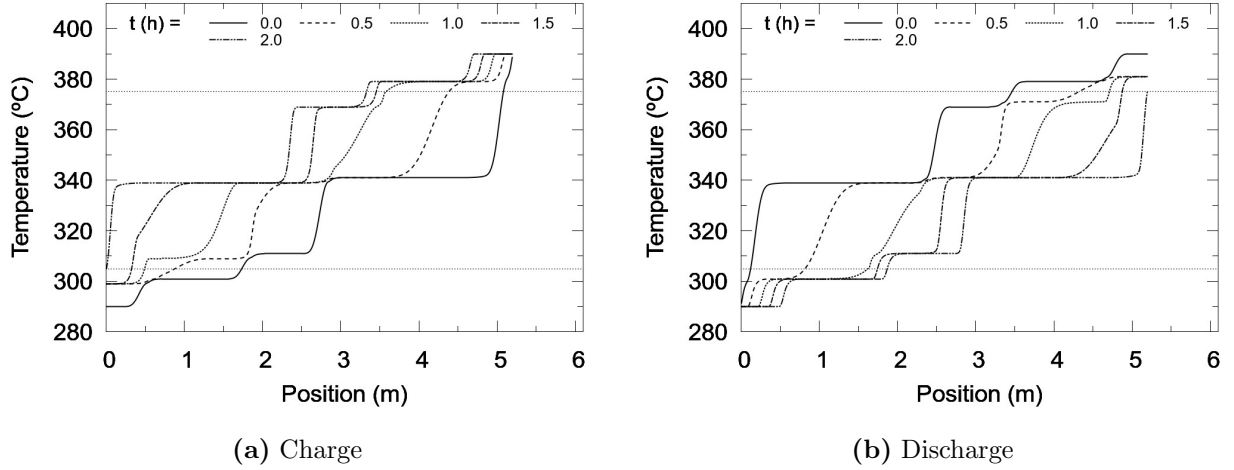


Figure 16: Case F2. Periodic state. Temperature maps at various instants. The chronological order of the curves is from right to left for the charge process and from left to right for the discharge.

3.2.5. Pressure losses

Pressure losses due to the presence of the filler material [first term on the right hand side of Eq. (6)] are below 400 Pa for all the cases studied. The highest losses are found in the thermocline

system filled uniquely with solid material (case A), due to the higher compactness of the solid filler material compared to those of the encapsulated PCMs. However, when compared against the pressure differences arising due to gravitational effects ($\rho gh \sim 1 \times 10^5$ Pa) these represent less than 0.4% in all the cases, and thus, are negligible.

4. Conclusions

A new multi-layered solid-PCM thermocline-like thermal storage concept for CSP plants has been presented. The key aspect of this new concept is the inclusion of PCM layers at both ends of the tank, whose fusion temperatures are conveniently chosen to lie inside the predefined admissible temperature ranges for the outgoing fluid in both charge and discharge processes. These admissible temperature ranges depend on the requirements of the power generation block and the solar receivers. The PCM layers act as thermal buffers, causing the outlet fluid to remain close to their melting points, and therefore inside the admissible temperature range for the corresponding process.

In order to design and evaluate the performance of such storage devices, as well as of the other thermocline-like systems considered, a numerical model has been developed and implemented. This model has been successfully validated against experimental data.

Several simulations have been carried out for different designs of thermocline tanks, where configurations of solid, single-PCM, multi-layered solid-PCM and cascaded PCM filler material configurations have been tested. The obtained results show that the multi-layered solid-PCM concept prevents from the high thermocline degradation presented by the pure thermocline, resulting in a much higher efficiency in the use of the overall thermal capacity of the system. Furthermore, compared against the cascaded PCM concept, this new approach has the advantage of using much less encapsulated PCM for almost the same total stored energy, again with a higher thermal efficiency. For example, prototype C4 (MLSPCM) stores around 83% of the energy stored with prototype F1 (cascaded PCM), using only 20% of the mass of PCM and 72% of molten salt; which is a consequence of being more efficient in the use of the storage capacity (84% vs. 65%, respectively).

Therefore, the MLSPCM thermocline storage systems can be considered as a promising solution for their use in CSP plants.

Acknowledgments

This work has been financially supported by the *Ministerio de Economía y Competitividad, Secretaría de Estado de Investigación, Desarrollo e Innovación*, Spain (ENE-2011-28699), by the EIT via the KIC InnoEnergy TESCONSOL project (ref. 20_2011_IP16) and by the *Secretaria d'Universitats*

i Recerca (SUR) del Departament d'Economia i Coneixement (ECO) de la Generalitat de Catalunya
and by the European Social Fund.

References

- [1] M. Medrano, A. Gil, I. Martorell, X. Potau, and L. F. Cabeza, "State of the art on high temperature thermal energy storage for power generation. part 2—Case studies," *Renew. Sust. Energy Rev.*, no. 14, pp. 56–72, 2010.
- [2] G. J. Kolb, C. K. Ho, T. R. Mancini, and J. A. Gary, "Power tower technology roadmap and cost reduction plan," Tech. Rep. SAND2011-2419, Sandia National Laboratories, 2011.
- [3] U. Herrmann, B. Kelly, and H. Price, "Two-tank molten salt storage for parabolic trough solar power plants," *Energy*, vol. 29, pp. 883–893, 2004.
- [4] J. I. Ortega, J. I. Burgaleta, and F. M. Téllez, "Central receiver system solar power plant using molten salt as heat transfer fluid," *J. Sol. Energy.-T. ASME*, vol. 130, pp. 024501–1–6, 2008.
- [5] J. E. Pacheco, S. K. Showalter, and W. J. Kolb, "Development of a molten-salt thermocline thermal storage system for parabolic trough plants," *J. Sol. Energy.-T. ASME*, vol. 124, pp. 153–159, 2002.
- [6] A. Yang and S. V. Garimella, "Molten-salt thermal energy storage in thermoclines under different environmental boundary conditions," *Appl. Energy*, vol. 87, pp. 3322–3329, 2010.
- [7] R. Tamme, D. Laing, and W. D. Steinmann, "Advanced thermal energy storage technology for parabolic trough," *J. Sol. Energy.-T. ASME*, vol. 126, pp. 794–800, 2004.
- [8] N. Calvet, J. C. Gomez, A. Faik, V. V. Roddatis, A. Meffre, G. C. Glatzmaier, S. Doppiu, and X. Py, "Compatibility of a post-industrial ceramic with nitrate molten salts for use as filler material in a thermocline storage system," *Appl. Energy*, vol. 109, pp. 387–393, 2013.
- [9] J. L. Shyu, R.J. and L. Fang, "Thermal analysis of stratified storage tanks," *J. Sol. Energy.-T. ASME*, vol. 111, pp. 54–61, 1989.
- [10] I. Rodríguez, J. Castro, C. Pérez-Segarra, and A. Oliva, "Unsteady numerical simulation of the cooling process of vertical storage tanks under laminar natural convection," *Int. J. Therm. Sci.*, vol. 48, pp. 708–721, 2009.
- [11] L. J. Shah and S. Furbo, "Entrance effects in solar storage tanks," *Sol. Energy*, vol. 75, pp. 337–348, 2003.

- [12] M. Liu, W. Saman, and F. Bruno, “Review on storage materials and thermal performance enhancement techniques for high temperature phase change thermal storage systems,” *Renew. Sust. Energ. Rev.*, vol. 16, pp. 2118–2132, 2012.
- [13] H. Michels and R. Pitz-Paal, “Cascaded latent heat storage for parabolic trough solar power plants,” *Sol. Energy*, vol. 81, pp. 829–837, 2007.
- [14] H. Shabgard, C. W. Robak, T. L. Bergman, and A. Faghri, “Heat transfer and exergy analysis of cascaded latent heat storage with gravity-assisted heat pipes for concentrating solar power applications,” *Sol. Energy*, vol. 86, no. 3, pp. 816–830, 2012.
- [15] K. Nithyanandam, R. Pitchumani, and A. Mathur, “Analysis of a latent thermocline storage system with encapsulated phase change materials for concentrating solar power,” *Appl. Energ.*, vol. 113, pp. 1446–1460, 2014.
- [16] S. M. Flueckiger and S. V. Garimella, “Latent heat augmentation of thermocline energy storage for concentrating solar power —A system-level assessment,” *Appl. Energ.*, vol. 116, pp. 278–287, 2014.
- [17] W. Steinmann and R. Tamme, “Latent heat storage for solar steam systems,” *J. Sol. Energ.-T. ASME*, vol. 130, pp. 011004–1–011004–5, 2008.
- [18] K. A. R. Ismail and R. Stuginsky Jr., “A parametric study on possible fixed bed models for pcm and sensible heat storage,” *Appl. Therm. Eng.*, vol. 19, pp. 757–788, 1999.
- [19] S. M. Flueckiger, Y. Z., and S. V. Garimella, “Review of molten-salt thermocline tank modeling for solar thermal energy storage,” *Heat Transfer Eng.*, vol. 34, no. 10, pp. 787–800, 2013.
- [20] C. Xu, Z. Wang, Y. He, X. Li, and F. Bai, “Sensitivity analysis of the numerical study on the thermal performance of a packed-bed molten salt thermocline thermal storage system,” *Appl. Energ.*, vol. 92, pp. 65–75, 2012.
- [21] A. Modi and C. D. Pérez-Segarra, “Thermocline thermal storage systems for concentrated solar power plants: One-dimensional numerical model and comparative analysis,” *Sol. Energy*, vol. 100, pp. 84–93, 2014.
- [22] J. P. Bédérrecats, J. Castaing-Lasvignottes, F. Strub, and J. P. Dumas, “Study of a phase change energy storage using spherical capsules. Part II: Numerical modelling,” *Energ. Convers. Manage.*, vol. 50, pp. 2537–2546, 2009.

- [23] A. Felix Regin, S. C. Solanki, and J. S. Saini, “An analysis of a packed bed latent heat thermal energy storage system using PCM capsules: Numerical investigation,” *Renew. Energ.*, vol. 34, pp. 1765–1773, 2009.
- [24] S. Karthikeyan and R. Velraj, “Numerical investigation of packed bed storage unit filled with PCM encapsulated spherical containers —A comparison between various mathematical models,” *Int. J. Therm. Sci.*, vol. 60, pp. 153–160, 2012.
- [25] P. Galione, C. D. Pérez-Segarra, I. Rodríguez, O. Lehmkuhl, and J. Rigola, “A new thermocline-PCM thermal storage concept for CSP plants. Numerical analysis and perspectives,” in *Proceedings of the SolarPACES 2013 International Conference*, vol. 49 of *Energy Procedia*, pp. 790–799, Elsevier, 2014.
- [26] G. Zanganeh, M. Commerford, A. Haselbacher, A. Pedretti, and A. Steinfeld, “Stabilization of the outflow temperature of a packed-bed thermal energy storage by combining rocks with phase change materials,” *Appl. Therm. Eng.*, no. 70, pp. 316–320, 2014.
- [27] N. Wakao, S. Kaguei, and T. Funazkri, “Effect of fluid dispersion coefficients on particle-to-fluid heat transfer coefficients in packed beds,” *Chem. Eng. Sci.*, vol. 34, pp. 325–336, 1979.
- [28] R. Krupiczka, “Analysis of thermal conductivity in granular materials,” *Int. Chem. Eng.*, vol. 7, no. 1, pp. 122–144, 1967.
- [29] A. Nakayama, F. Kuwahara, and Y. Kodama, “An equation for thermal dispersion flux transport and its mathematical modelling for heat and fluid flow in a porous medium,” *J. Fluid Mech.*, vol. 563, pp. 81–96, 2006.
- [30] R. G. Holdich, *Fundamentals of particle technology*. Midland Information Technology and Publishing, 2002.
- [31] F. J. Oppel, A. J. Ghajar, and P. M. Moretti, “Computer simulation of stratified heat storage,” *Appl. Energ.*, vol. 23, pp. 205–224, 1986.
- [32] S. M. Flueckiger, B. D. Iverson, S. V. Garimella, and J. E. Pacheco, “System-level simulation of a solar power tower plant with thermocline thermal energy storage,” *Appl. Energ.*, vol. 113, pp. 86–96, 2014.
- [33] N. Nallusamy, S. Sampath, and R. Velraj, “Experimental investigation on a combined sensible and latent heat storage system integrated with constant/varying (solar) heat sources,” *Renew. Energ.*, vol. 32, pp. 1206–1227, 2007.

623 [34] A. B. Zavoico, “Solar power tower design basis document,” Tech. Rep. SAND2001-2100, Sandia
624 National Laboratories, 2001.